

Quasi-localization dynamics in a Fibonacci quantum rotor

Sourav Bhattacharjee,* Souvik Bandyopadhyay, and Amit Dutta
Department of Physics, Indian Institute of Technology Kanpur, Kanpur 208016, India

The dynamics of a quantum kicked rotor(QKR), unlike that of its classical counterpart, is known to be non-ergodic. This is due to the emergence of a dynamically localized wave-function in the angular momentum space, courtesy of interference affects. In this work, we analyze the dynamics of a quantum rotor kicked with a binary Fibonacci sequence of two distinct drive amplitudes. While the dynamics at low drive frequencies is found to be diffusive, a long-lived pre-ergodic regime emerges in the other limit. The dynamics in this pre-ergodic regime mimics that of a regular QKR and can be associated with the onset of a dynamical quasi-localization. We establish that this peculiar behavior arises due to the presence of localized eigenstates of an approximately conserved effective Hamiltonian, which drives the evolution at Fibonacci instants. However, the effective Hamiltonian picture does not persist indefinitely and the dynamics eventually becomes ergodic after asymptotically long times.

I. INTRODUCTION

The quantum kicked rotor (QKR) [1, 2] has been subjected to a plethora of analytical [3–8] as well as experimental [9–15] investigations over the years, with an aim to demystify the principles of quantum chaos [16–18]. The dynamics of its classical version, which displays both regular and chaotic behavior, has been extensively studied. The QKR, on the contrary, seemingly exhibits a non-ergodic behavior owing to quantum interference effects. The wave-function is found to be *dynamically localized* in the angular momentum space; the energy pumped into the rotor over time thus saturates, rather than heating up indefinitely. In contrast to the classical rotor, this non-ergodicity in the dynamics is manifested for any finite amplitude and frequency of the kicks (see appendix A for a brief recapitulation) . Further, the localization dynamics of the QKR in the momentum space can be mapped to the Anderson localization problem [19] in one-dimensional real space [4, 5], the latter is commonly studied in a one-dimensional lattice system subjected to a pseudo-random potential in space. This mapping thus provides an analytical justification of the dynamical localization observed in the temporal evolution of the QKR.

It is well known that the Anderson problem in more than one spatial dimension exhibits a localization-delocalization transition [20], with the two dimensional situation being the marginal case. Attempts to observe a similar transition in the dynamics of the QKR have thus focused on increasing the temporal dimension of the rotor Hamiltonian [21], i.e., by superimposing additional temporal modulations on the drive. As for example, it has been observed that the dynamics of a QKR driven with three incommensurate frequencies can be mapped to the three dimensional Anderson problem and thus can exhibit both dynamical localization as well as diffusive growth in its kinetic energy [22]. Similarly, the localiza-

tion as well as delocalization behavior has been reported in coupled systems of multiple kicked rotors [23–29]. Finally, the robustness of the dynamically localized phase when subjected to a multitude of perturbations such as noise and environment induced dissipation effects have also been actively investigated [13–15, 30–35].

It is also important to note that in the conventional QKR, the periodicity of the external drive implies that the effective Floquet Hamiltonian [36–39] is a conserved quantity at all stroboscopic instants of time. Further, the eigen-states of the Floquet Hamiltonian are found to be exponentially localized in the momentum space, which ultimately leads to the localization of the rotor dynamics. A similar Floquet structure also emerges in the case of a QKR driven with three incommensurate frequencies – the rotor Hamiltonian with time dependent kick amplitude is first mapped to a three dimensional rotor (albeit with the kinetic energy being linear in momentum in two of the three orthogonal directions) with time-independent kick amplitudes at equal time intervals [22]. The temporal evolution at stroboscopic intervals is then found to be governed by a Floquet propagator as in the conventional QKR. In the localized phase, all the eigenstates are found to be localized in the momentum space while all of them are found to be extended in the delocalized phase. Generically (see Ref. 40), although quantum systems driven simultaneously with multiple incommensurate frequencies do not allow a Floquet description, they can be approximated by effective periodic drives with excellent convergence. This is possible because of the existence of rational fractions (also known as metallic means) which lie arbitrarily close to irrational numbers on the number line.

Recently, the Fibonacci drive (also known as Thue-Morse sequence) [41–43] has been extensively used to impose and explore the consequences of quasi-periodicity in the time domain in various out-of-equilibrium systems [44–50]. The Fibonacci drive, by its definition, has a unique self-similar structure which can significantly affect the dynamics. Interestingly, it also possesses dynamical invariants which add to the rich physics of dynamical quasiperiodic systems[51–54]. Moreover, to the best of

* sourav.offc@gmail.com

our knowledge, a straightforward way of approximating the quasi-periodicity imposed by Fibonacci drives with effective periodic drives, except at asymptotically long stroboscopic times does not exist. It therefore becomes imperative to investigate how the dynamics of a QKR is modified when kicked with a Fibonacci drive in stead of regular periodic drive.

With the above motivation in mind, we propose a new variant of the QKR, dubbed as the *Fibonacci quantum kicked rotor* (FQKR), where the kick amplitudes at subsequent stroboscopic instants follow a binary Fibonacci sequence. It is important to note that one can not associate any conserved Floquet Hamiltonian *per se* as in the case of the conventional QKR which drives the evolution. Remarkably, we however find that while the dynamics at low drive frequencies is ergodic, a ‘pre-ergodic’ regime emerges in the limit of high frequencies during which the wave-function of the FQKR remains ‘dynamically quasi-localized’ in the angular momentum space. Although the dynamics eventually becomes ergodic, the pre-ergodic regime persists over a significant period of time of experimental relevance, which progressively becomes longer as the frequency of the drive is further increased.

We would like to emphasize here that although the Fibonacci drive is inherently a quasi-periodic sequence, the approach of our work is distinct from those studied previously in literature [22, 55], where quasi-periodicity is enforced by driving the rotor at incommensurate frequencies. On the contrary, in our case, quasi-periodicity is imbibed in the sequence of the (binary) kick amplitudes driving the system. As we shall show below, the quasi-localization observed in the pre-ergodic regime is not discernible from a standard Floquet analysis of the evolution operator. Rather, it follows from the existence of *self-similar eigenstates* and is thus different from hitherto observed dynamical localization in the conventional QKR.

At this point it would be imperative to note that the existence of a pre-ergodic regime is unique to the FQKR and is may not be found for any arbitrary binary sequence. As for example, we show in Appendix. B that a periodic binary sequence (bi-periodic) leads to qualitatively the same dynamics as in the case of a conventional QKR while an aperiodic binary sequence leads to ergodic behavior at all times for all frequencies. However, we note that the existence of a pre-ergodic regime can not be ruled out for other types of quasi-periodic binary sequences.

The rest of the paper is organized as follows. The dynamics of the QKR is briefly discussed in Sec. II. Numerical results demonstrating the dynamics of the FQKR is discussed in Sec. III. The dynamical quasi-localization observed in the high frequency limit of the FQKR is established through a perturbative expansion of the unitary evolution operator in Sec. IV. Further, analytical evidence of the onset of diffusion at lower frequencies is also

extracted from the perturbative expansion. Summary of the work and future outlook is discussed in Sec. V. In addition, three appendices are also included for the benefit of the reader. Appendix. A a brief discussion on the factors leading to dynamical localization in a regular QKR is recapitulated. For a comparative analysis, the dynamics of a QKR kicked with *bi-periodic* and *aperiodic* binary sequences are discussed in Appendix. B. Explicit calculations of the high frequency perturbative expansion of the unitary evolution operator are provided in Appendix. C.

II. MODEL

The QKR is represented by the Hamiltonian,

$$H(t) = \frac{\hat{l}^2}{2I} + \cos \hat{\theta} \sum_{N=0}^{\infty} K_N \delta(t - NT), \quad (1)$$

where $\hat{\theta}$ and \hat{l} are the angular displacement and angular momentum operators, respectively, while I is the moment of inertia of the rotor. Note that \hat{l} satisfies $\hat{l}|l\rangle = \hbar l|l\rangle$, where $\{|l\rangle\}$ are the angular momentum eigenstates with $l \in \mathbb{Z}$. The rotor evolves freely with time period T between subsequent kicks of strength K_N , which act on the rotor at the stroboscopic instants NT , where $n \in \mathbb{Z}^+$. We note that for a regular QKR, $K_N = \text{constant}, \forall N$. However, in our case, we consider $K_N \in \{K_1, K_2\}$ and thus $\{K_N\}_{n=1}^{\infty} \equiv K_1, K_2, \dots$ constitutes a binary sequence.

In what follows, we shall be concerned with the evolved state of the QKR at stroboscopic instants, just prior to each of the kicks. If the rotor is initially in a state $|\psi(t=0)\rangle = |\psi_0\rangle$, the state of the system just before the N^{th} kick is thus given by,

$$|\psi_N\rangle \equiv |\psi(NT)\rangle = U(NT, 0)|\psi_0\rangle = U_N U_{N-1} \dots U_1 |\psi_0\rangle, \quad (2)$$

U_N being the the unitary operator propagating the system from the $(N-1)^{\text{th}}$ to N^{th} time interval given by,

$$U_N = \mathcal{T} \exp \left(-\frac{i}{\hbar} \int_{(N-1)T}^{NT} H(t) dt \right) = e^{-i\frac{\hat{l}^2}{2}\tau} e^{-iK_N \cos \hat{\theta}}, \quad (3)$$

where \mathcal{T} is the time-ordering operator. Note that we have set $\hbar = 1$ and rescaled the time-period T to a dimensionless parameter $\tau = T/I$. In particular, we shall be interested in tracking the temporal evolution of the kinetic energy $\langle \hat{l}^2 \rangle$ at stroboscopic instants, where the expectation is calculated over the time-evolved state of the rotor.

A. Conventional QKR

The conventional QKR can be recovered from the binary sequence by setting $K_N = \mathcal{K}$ for all N . The dynamics is then equivalent to an evolution under the Floquet

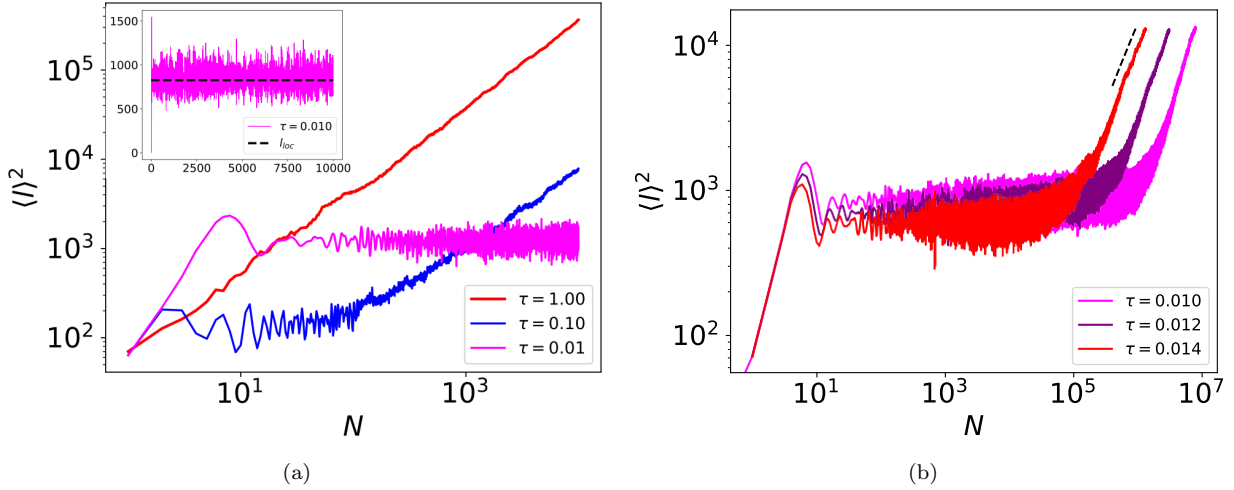


FIG. 1. (a) The kinetic energy of a FQKR grows diffusively at lower drive frequencies and dynamically quasi-localizes at high frequency ($\tau < 0.1$). The inset shows that the fluctuations in the quasi-localized (pre-ergodic) regime are evenly spread about the mean kinetic energy calculated from the perturbation analysis (black dashed line) in Eq. (14). (b) The quasi-localization is destroyed and an ergodic behavior is found to emerge at very long times. This can be seen from the linear growth of the kinetic energy with unit slope for $N > 10^5$. The (black) dashed line with unit slope is provided for reference. Further, the time after which localization is destroyed progressively increases as the frequency (τ^{-1}) is increased. The kick amplitudes chosen for the plot are $\mathcal{K}_1 = 10$, $\mathcal{K}_2 = 12$ and the initial state is chosen to be the angular momentum eigenstate $|\psi_0\rangle = |l=0\rangle$.

propagator $U_F = e^{-i\frac{l^2}{2}\tau} e^{-i\mathcal{K}\cos\hat{\theta}}$, such that Eq. (2) can be written as,

$$|\psi_N\rangle = (U_F)^N |\psi_0\rangle. \quad (4)$$

For a finite \mathcal{K} , the eigenstates of U_F are exponentially localized in the angular momentum space. Thus, any given initial state only ‘sees’ or overlaps with a finite number of these eigenstates l_s . The Floquet spectrum, being bounded modulo 2π , is thus effectively discrete with a mean density $2\pi/l_s$. The system requires a finite time, referred to as the Heisenberg time, to reach a stationary value (see Appendix A for details), during which the momentum grows diffusively.

B. Fibonacci QKR

We define the FQKR as a quantum rotor evolving with the Hamiltonian in (1), where the sequence of kicks follows the Fibonacci sequence,

$$K_N = \mathcal{K}_1 + (2 - \gamma(N)) \frac{\Delta\mathcal{K}}{2}, \quad (5a)$$

where $\Delta\mathcal{K} = \mathcal{K}_2 - \mathcal{K}_1$. The generating function $\gamma(N)$ can assume the values 0 or 2 and is given by,

$$\gamma(N) = \lfloor (N+1)G \rfloor - \lfloor NG \rfloor, \quad (5b)$$

where $\lfloor x \rfloor$ denotes the greatest integer less than or equal to x and G is the golden mean: $G = (\sqrt{5} + 1)/2$. To see that Eq. (5) generates a Fibonacci sequence, let us look at the sequences generated at Fibonacci instants of kicks.

Let us denote the number of stroboscopic instants corresponding to the \mathcal{N}^{th} Fibonacci instant as $F(\mathcal{N})$, such that $F(1) = 1$, $F(2) = 2$, $F(3) = 3$, $F(4) = 5$, $F(6) = 8$, $F(7) = 13$, and so on. Note that $F(\mathcal{N})$ satisfies the Fibonacci rule $F(\mathcal{N}) = F(\mathcal{N}-1) + F(\mathcal{N}-2)$. Assuming that $K_1 = \mathcal{K}_1$, we have,

$$\begin{aligned} (K_N)_{N=1}^{F(1)} &: S_1 = \mathcal{K}_1 \\ (K_N)_{N=1}^{F(2)} &: S_2 = \mathcal{K}_1 \mathcal{K}_2 \\ (K_N)_{N=1}^{F(3)} &: S_3 = \mathcal{K}_1 \mathcal{K}_2 \mathcal{K}_1 \\ (K_N)_{N=1}^{F(4)} &: S_4 = \mathcal{K}_1 \mathcal{K}_2 \mathcal{K}_1 \mathcal{K}_1 \mathcal{K}_2 \\ (K_N)_{N=1}^{F(5)} &: S_5 = \mathcal{K}_1 \mathcal{K}_2 \mathcal{K}_1 \mathcal{K}_1 \mathcal{K}_2 \mathcal{K}_1 \mathcal{K}_2 \mathcal{K}_1 \\ (K_N)_{N=1}^{F(6)} &: S_6 = \mathcal{K}_1 \mathcal{K}_2 \mathcal{K}_1 \mathcal{K}_1 \mathcal{K}_2 \mathcal{K}_1 \mathcal{K}_2 \mathcal{K}_1 \\ &\quad \mathcal{K}_1 \mathcal{K}_2 \mathcal{K}_1 \mathcal{K}_1 \mathcal{K}_2, \end{aligned} \quad (6)$$

where S_n denotes the n^{th} Fibonacci sequence, satisfying $S_n = S_{n-1}S_{n-2}$.

In the next section, we shall discuss the dynamical evolution of the FQKR and its dependence on the driving frequencies. Unless mentioned otherwise, the initial state is chosen to be a normalized Gaussian wave-packet centered around the angular momentum l_0 ,

$$\psi_0(l) = \left(\frac{2}{\pi}\right)^{\frac{1}{4}} e^{-(l-l_0)^2} \quad (7)$$

Further, we employ a truncated basis of angular momentum states for the numerics so that $(l_0 - S/2) \leq l \leq (l_0 + S/2 - 1)$, where S is chosen to be large enough to ensure normalization of the wave function at all times.

For dynamical localized wave-functions, this is ensured by choosing $S \gg \xi$, where ξ is the localization length. For wave-functions evolving diffusively starting from the initial state $\psi_0(l)$, the size of the basis is adjusted as per the maximum time to which the system is observed. The dynamics is probed by observing the evolution of the average kinetic energy $\propto \langle l^2 \rangle$.

III. NUMERICAL RESULTS

The temporal evolution of the kinetic energy $\langle l^2 \rangle$ for the FQKR is shown in Fig. 1(a). We find that the kinetic energy grows diffusively at low frequencies (high τ) and localizes at high, but finite frequency $\tau \leq 0.01$. However, as shown in Fig. 1(b), the localization does not persist indefinitely and a diffusive behavior emerges eventually. Nevertheless, the time after which this happens rapidly increases as the drive frequency increases. We have numerically verified that the results remain qualitatively the same for different choices of \mathcal{K}_1 and \mathcal{K}_2 .

Interestingly, the quasi-localization observed at high frequencies is analogous to the *prethermal* regimes found in out-of-equilibrium many-body quantum systems. In such systems, the presence of approximately conserved quantities prevent the system from thermalizing for a long period of time. Similarly, the quasi-localization observed in the case of FQKR can be associated with the existence of a *pre-ergodic* regime. In the next section, we will show that one can also identify an approximately conserved effective Hamiltonian with localized eigenstates at high frequencies which lies at the root of the observed quasi-localized dynamics.

IV. PERTURBATIVE ANALYSIS IN THE LIMIT OF HIGH FREQUENCY

In this section, we resort to a perturbative analysis of the unitary evolution operator, with $\tau = T/I$ as the small parameter, to corroborate the numerical results presented in Sec. III. As we shall illustrate below, the perturbative analysis not only establishes the existence of observed quasi-localization in the case of the FQKR, but also points to the crossover to a diffusive behavior at low frequencies.

A. Perturbative expansion of the evolution operator

For $\tau \ll 1$, the unitary operator U_N driving the evolution between the $(N-1)^{th}$ and N^{th} kicks can be written as,

$$U_N = e^{-i\frac{l^2}{2}\tau} e^{-iK_N \cos \hat{\theta}} \approx e^{-iL_{1,2}}, \quad (8a)$$

where $L_{1,2}$ is calculated from a Baker-Campbell-Hausdorff (BCH) expansion of U_N ,

$$L_{1,2} = \mathcal{K}_{1,2} \cos \hat{\theta} + \frac{\tau}{2} \left[\hat{l}^2 + \frac{\mathcal{K}_{1,2}}{2} (\hat{l} \sin(\hat{\theta}) + \sin(\hat{\theta}) \hat{l}) \right. \\ \left. + \frac{\mathcal{K}_{1,2}^2}{12} \sin^2(\hat{\theta}) \right] + \mathcal{O}(\tau^2), \quad (8b)$$

where we have retained terms only up to linear order in τ . By successively operating with the time-evolution operator for each period, it can be shown (see Appendix C) that the evolution operator after N kicks assumes the form $U_N = e^{-iH_N N}$, where the effective Hamiltonian H_N takes the form,

$$H_N = \frac{\alpha(N)}{N} L_1 + \frac{\beta(N)}{N} L_2 + \frac{\delta(N)}{N} [L_2, L_1] \\ + \frac{\eta_1(N)}{N} [L_1, [L_1, L_2]] + \frac{\eta_2(N)}{N} [L_2, [L_2, L_1]] + \mathcal{O}(\tau^2), \quad (9)$$

where the quantities $\alpha(N)$, $\beta(N)$, $\delta(N)$, $\eta_1(N)$ and $\eta_2(N)$ are determined by the exact form of the binary sequence. We shall henceforth collectively refer to these quantities as *expansion coefficients*, or *normalized expansion coefficients* (NEC) when divided by N , of the effective Floquet Hamiltonian. Notably, all other higher order commutators in the BCH expansion contributes terms which are at least quadratic in τ and hence has been ignored in the above expression.

For the Fibonacci sequence, the expansion coefficients can be computed as follows (see Appendix C),

$$\beta(N) = \sum_{n=1}^N (2 - \gamma(n)), \quad (10a)$$

$$\alpha(N) = \sum_{n=1}^N (\gamma(n) - 1) = N - \beta(N). \quad (10b)$$

$$\delta(N) = -\frac{1}{2} \sum_{n=1}^N \left[(\gamma(n) - 1)(n - 1) - \left\lfloor \frac{nG}{1+G} \right\rfloor \right], \quad (10c)$$

$$\eta_1(N) = \frac{1}{12} \sum_{n=1}^N \left[(2 - \gamma(n)) \left\lfloor \frac{nG}{1+G} \right\rfloor^2 \right. \\ \left. + (1 - \gamma(n)) \left(6\delta(n-1) - (2-n) \left\lfloor \frac{n}{1+G} \right\rfloor - \left\lfloor \frac{n}{1+G} \right\rfloor^2 \right) \right], \quad (10d)$$

$$\eta_2(N) = \frac{1}{12} \sum_{n=1}^N \left[(\gamma(n) - 1) \left\lfloor \frac{n}{1+G} \right\rfloor^2 \right. \\ \left. + (2 - \gamma(n)) \left(6\delta(n-1) + (2-n) \left\lfloor \frac{nG}{1+G} \right\rfloor + \left\lfloor \frac{nG}{1+G} \right\rfloor^2 \right) \right]. \quad (10e)$$

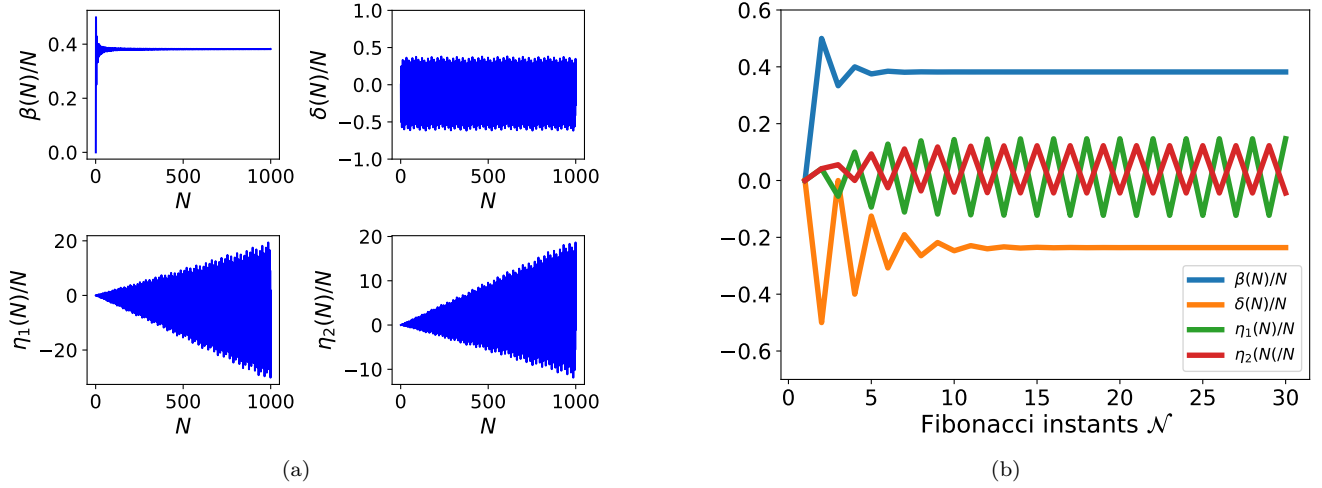


FIG. 2. The normalized expansion coefficients given in Eq. (10) as a function of (a) stroboscopic and (b) Fibonacci instants.

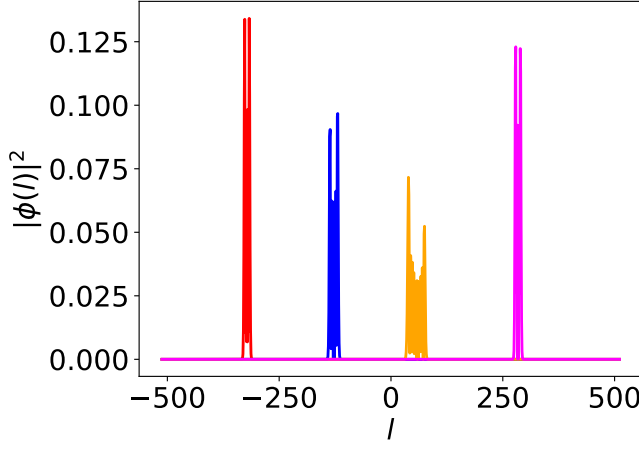


FIG. 3. Typical eigenstates of U_{fi} , defined in Eq. (12) with $\mathcal{K}_1 = 10$, $\mathcal{K}_2 = 12$ and $\tau = 0.01$. The eigenstates are found to be localized in the angular momentum space.

In the above set of equations, $G = (\sqrt{5} + 1)/2$ is the golden ratio and $\lfloor x \rfloor$ denotes the greatest integer less than or equal to x . The function $\gamma(n) = \lfloor (n+1)G \rfloor - \lfloor nG \rfloor$ is the generator of the binary Fibonacci sequence defined in Eq. (6) (see Appendix C).

Fig. 2(a) shows the temporal variation of the NECs, computed using Eq. (10). We see that while $\beta(N)/N$ (and hence $\alpha(N)/N = 1 - \beta(N)/N$) saturates to a constant value, $\delta(N)/N$ exhibits small amplitude fluctuations about a mean value. On the other hand, the growth of the coefficients $\eta_1(N)/N$ and $\eta_2(N)/N$ with N is unbounded. The effective Hamiltonian H_N , as defined in Eq. (9), is therefore N - dependent and no effective Floquet Hamiltonian can thus be identified. However, a different picture emerges if we observe the behavior of the expansion coefficients at Fibonacci instants \mathcal{N} .

As shown in Fig. 2(b), the coefficients $\beta(F(\mathcal{N}))/F(\mathcal{N})$,

$\alpha(F(\mathcal{N}))/F(\mathcal{N})$ and $\delta(F(\mathcal{N}))/F(\mathcal{N})$ are found to saturate to steady values for $\mathcal{N} > 10$ while the coefficients $\eta_1(F(\mathcal{N}))/F(\mathcal{N})$ and $\eta_2(F(\mathcal{N}))/F(\mathcal{N})$ oscillate between a pair of constant values. Indeed, using the so-called ‘local deflation rule’ for the Fibonacci sequence, one can show that the asymptotic values of the NECs for $\mathcal{N} \gg 1$ are given by[56],

$$\frac{\alpha(F(\mathcal{N}))}{F(\mathcal{N})} = \frac{1}{G} \quad (11a)$$

$$\frac{\beta(F(\mathcal{N}))}{F(\mathcal{N})} = \frac{1}{G^2} \quad (11b)$$

$$\frac{\delta(F(\mathcal{N}))}{F(\mathcal{N})} = -\frac{1}{G^3} \quad (11c)$$

$$\frac{\eta_1(F(\mathcal{N}))}{F(\mathcal{N})} = \frac{1}{12} \left[\frac{1}{G^4} + (-1)^{\mathcal{N}} \left(\frac{2}{G} + \frac{1}{G^2} \right) \right] \quad (11d)$$

$$\frac{\eta_2(F(\mathcal{N}))}{F(\mathcal{N})} = \frac{1}{12} \left[\frac{1}{G^5} - (-1)^{\mathcal{N}} \left(\frac{2}{G^2} + \frac{1}{G^3} \right) + \frac{1}{G^2} \right] \quad (11e)$$

We shall henceforth denote the saturation values of the NECs at Fibonacci instants as $\bar{\alpha}$, $\bar{\beta}$, $\bar{\delta}$, $\bar{\eta}_1$, $\bar{\eta}_2$, where $\bar{\eta}_1$ and $\bar{\eta}_2$ correspond to the mean of the oscillating values of $\eta_1(N)/N$ and $\eta_2(N)/N$, respectively.

B. Localization in the high frequency limit

Substituting the saturation values defined above in Eq. (9), the propagator at Fibonacci instants $U_{F(\mathcal{N})}$ can be expressed in terms of an *effective Fibonacci propagator* U_{fi} , such that,

$$U_{N=F(\mathcal{N})} \approx U_{fi}^{F(\mathcal{N})} = e^{-iH_{fi}F(\mathcal{N})} \quad (12a)$$

where,

$$H_{fi} = \bar{\alpha}L_1 + \bar{\beta}L_2 + \bar{\delta}[L_2, L_1] + \bar{\eta}_1[L_1, [L_1, L_2]] + \bar{\eta}_2[L_2, [L_2, L_1]], \quad (12b)$$

is defined as the *effective Fibonacci Hamiltonian*. As shown in Fig. IV A, the eigenstates of U_{fi} are localized in the angular momentum basis. Arguing as in the case of the conventional QKR, we therefore conclude that the wave-function remains localized when observed at Fibonacci instants $N = F(\mathcal{N})$. Nevertheless, the existence of an effective Floquet Hamiltonian at Fibonacci instants of kicks does not explain the persistent localization seen throughout the evolution. In other words, we are yet to ascertain what causes the wave-function to remain localized in between two Fibonacci instants, i.e. for $F(\mathcal{N}) < N < F(\mathcal{N}+1)$. The localization appears particularly surprising, given that the growth of the coefficients $\eta_1(N)/N$ and $\eta_2(N)/N$ are unbounded when observed at stroboscopic instants, as can be seen in Fig. 2(a).

The apparent contradiction can be explained if one inspects the self-similar or fractal nature of the Fibonacci sequence. To elaborate, let us consider the evolution between two subsequent Fibonacci instants \mathcal{N}^* and \mathcal{N}^*+1 , where we have assumed $F(\mathcal{N}^*) \gg 1$ so as to ensure that the NECs have saturated to their mean values (η_1 and η_2 oscillate about their respective mean values). From Eq. (6), we note that the sequence of kicks up to $N = F(\mathcal{N}^*)$ and $N = F(\mathcal{N}^*+1)$ is given by $S_{\mathcal{N}^*}$ and $S_{\mathcal{N}^*+1}$, respectively. However, by construction, we have $S_{\mathcal{N}^*+1} = S_{\mathcal{N}^*}S_{\mathcal{N}^*-1}$, which immediately implies that the sequence of kicks between $N = F(\mathcal{N}^*)$ and $N = F(\mathcal{N}^*+1)$ is nothing but the sequence $S_{\mathcal{N}^*-1}$.

Using the above insight, we now argue as follows. Given a localized wave-function $|\psi_{N^*}\rangle$, where $N^* = F(\mathcal{N}^*)$, the wave-function at the instants $N^* + F(1)$, $N^* + F(2)$, $N^* + F(3)$, \dots , $N^* + F(\mathcal{N}^* - 1)$, is given by,

$$|\psi_{N^*+F(\mathcal{M})}\rangle \approx U_{fi}^{F(\mathcal{M})} |\psi_{N^*}\rangle, \quad (13)$$

where $\mathcal{M} = 0, 1, 2, 3, \dots, \mathcal{N}^* - 1$ denotes Fibonacci instants nested in between $N = F(\mathcal{N}^*)$ and $N = F(\mathcal{N}^* + 1)$. Hence, the wave-function also remains localized at the instants $N^* + F(\mathcal{M})$, being driven by the same effective Floquet Hamiltonian U_{fi} . Proceeding similarly, one can argue that the sequence of kicks acting between $N = N^* + F(\mathcal{M}^*)$ and $N^* + F(\mathcal{M}^* + 1)$ is precisely the sequence $S_{\mathcal{M}^*-1}$ and hence the wave-function remains localized at the Fibonacci instants nested between $N = N^* + F(\mathcal{M}^*)$ and $N^* + F(\mathcal{M}^* + 1)$.

It is thus clear that the localised eigenstates of U_{fi} , which can be regarded as *self-similar eigenstates* of U_N , lies at the origin of the quasi-localized dynamics. However, it is to be noted that the above arguments remain meaningful as long as the approximate equality in Eq. (12) is satisfied.

To further support the arguments presented above, we estimate the localization length $\langle \hat{l}^2 \rangle_{loc}$, with the initial state of the rotor is an angular momentum eigenstate, $|\psi_0\rangle = |l_0\rangle$, for simplicity in calculation. Assuming that, $|\psi_{F(\mathcal{N})}\rangle \approx U_{fi}^{F(\mathcal{N})} |l_0\rangle$ and $U_{fi} = VDV^\dagger$, where D is a diagonal matrix, we have (see Appendix A),

$$\langle \hat{l}^2 \rangle_{loc} = \sum_{l,m} l^2 |V_{l_0 m}|^2 |V_{l m}|^2 \quad (14)$$

As shown in the inset of Fig. 1(b), the fluctuations in the kinetic energy for $N < 10^4$ is indeed found to be evenly distributed about the mean value calculated using Eq. (14).

C. Emergence of diffusive behavior at low frequencies

Although the perturbative analysis discussed in the Sec. IV B is valid only in the limit of high frequency, we show below that the emergence of diffusive behavior at lower frequencies becomes evident if higher order terms are progressively included in the BCH expansion of the effective Hamiltonian in (9). In fact, such terms begin to contribute significantly as the frequency of quasi-periodic drive is lowered. In addition, we note that the terms of order $\mathcal{O}(\tau)$ in Eq. (12) are also modified with decreasing frequency (see Eq. (8b)).

Let us recall that the saturation of the NECs to steady values for $\mathcal{N} \gg 1$ is crucial for the existence of an effective Fibonacci Hamiltonian. Without explicitly determining all the commutator terms that may contribute when terms of order $\sim \mathcal{O}(\tau^2)$ are included, let us analyze the expansion coefficients of the commutators $[L_1, [L_1, [L_1, L_2]]]$, $[L_2, [L_2, [L_1, L_2]]]$ and $[L_1, [L_2, [L_1, L_2]]]$. We denote the corresponding expansion coefficients as $\mu_1(N)$, $\mu_2(N)$ and $\mu_3(N)$, respectively. These NECs at $N = F(\mathcal{N})$ with $\mathcal{N} \gg 1$ are given by [56],

$$\frac{\mu_1(F(\mathcal{N}))}{F(\mathcal{N})} = \frac{(-1)^{\mathcal{N}}}{120} \left[G^{\mathcal{N}-1} + \frac{1}{G} [(-1)^{\mathcal{N}} (3G - 4) - 1 - 3G] \right], \quad (15a)$$

$$\frac{\mu_2(F(\mathcal{N}))}{F(\mathcal{N})} = \frac{(-1)^{\mathcal{N}}}{120} \left[G^{\mathcal{N}-1} (2 - G) + \frac{1}{G} [(-1)^{\mathcal{N}} (4G - 7) - 2 - G] \right], \quad (15b)$$

$$\frac{\mu_3(F(\mathcal{N}))}{F(\mathcal{N})} = \frac{(-1)^{\mathcal{N}}}{120} \left[2G^{\mathcal{N}-1}(1-G) + \frac{1}{G} [(-1)^{\mathcal{N}}(3-G) + 3 + 4G] \right], \quad (15c)$$

where we have ignored terms of order $G^{-(\mathcal{N}+1)}$, $G^{-(2\mathcal{N}+1)}$, $G^{-(3\mathcal{N}+1)}$, etc.

It is immediately clear that the NECs defined above do not saturate to steady values even in the asymptotic limit, rather their growth with \mathcal{N} is unbounded. Indeed, it can be shown that this is true for all the NECs of higher order nested commutators [56]. Thus, we conclude that when the frequency of the drive is low enough such that the contribution of higher order terms become significant, the dynamics at Fibonacci instants is no longer governed by an effective Fibonacci Hamiltonian. The evolution of the rotor then mimics that of a randomly driven rotor, thereby leading to the emergence of ergodic behavior after sufficiently long times.

D. Crossover from pre-ergodic to ergodic regime

It has been established in Sec. IV C that the NECs of commutators arising from terms of order $\mathcal{O}(\tau^2)$ do not saturate to steady values and their growth is unbounded in \mathcal{N} . It is therefore to be expected that even for $\tau \ll 1$, there exists a finite time at which the higher order terms start to dominate the dynamics and consequently, the ergodic behavior sets in. Indeed, one can perform an order of magnitude estimation of the time N_{deloc} , after which the diffusive growth is expected to manifest as follows. From Eq. (15), we note that the leading order term which is unbounded in \mathcal{N} grows as $G^{\mathcal{N}}/120$. The $\mathcal{O}(\tau^2)$ terms in the expansion of Eq. (12b) thus become significant when $\tau^2 G^{\mathcal{N}_{deloc}}/120 \sim 1$. For $\tau \approx 0.01$, this translates to $\mathcal{N}_{deloc} \approx 29$ or $N_{deloc} \approx 1.3 \times 10^6$; Thus, within the experimentally realisable time scale, one should observe the quasi-localisation. This agrees remarkably well with the results found from exact numerical calculations (see Fig. 1(b)).

V. SUMMARY

To summarize, we have shown in this work that a quantum rotor driven with a binary Fibonacci sequence of two different amplitudes can exhibit both diffusive and quasi-localization behavior. In the low frequency regime, the dynamics of the rotor mimics that of a noisy QKR, as is seen from the linear unbounded growth of its kinetic energy. The situation is found to be completely different at high frequency regime, where the dynamics of the rotor resembles that of the regular QKR within the pre-ergodic regime. In this case, the kinetic energy quasi-localizes, signaling the onset of a dynamical quasi-localization. Thus, there exists a crossover from a diffusive to quasi-localized behavior as the frequency of the

drive is increased.

Unlike the case of a conventional QKR, the absence of any definite time-periodicity in the Hamiltonian of the FQKR implies that the non-ergodicity can no longer be attributed to the existence of the exponentially localized Floquet eigenstates. However, in the high frequency limit, a perturbative expansion of the unitary evolution operator reveals interesting details. In particular, we find that it is possible to identify a time-independent effective Fibonacci Hamiltonian, which drives the macro-motion of the rotor at Fibonacci instants. This is akin to the Floquet Hamiltonian, which drives the macro-motion of perfectly time-periodic Hamiltonians at stroboscopic instants. Further, the eigenstates of this effective Fibonacci Hamiltonian are found to be highly localized in the angular momentum space. This guarantees a localized behavior when the dynamics is observed only at Fibonacci instants of time. However, the self-similar structure of the Fibonacci sequence immediately implies that the evolution between any two consecutive Fibonacci instants is in fact driven by a fractal series of nested Fibonacci drives. Hence, the localization manifests not only when observed at Fibonacci instants but also at all stroboscopic instants of time within the pre-ergodic regime.

However, at lower frequencies, the interpretation of the dynamics in terms of an effective Fibonacci Hamiltonian breaks down when higher order terms in the perturbative expansion start to dominate. As a result, the dynamical quasi-localization observed at high frequencies is destroyed and the dynamics of the rotor becomes ergodic. The same also happens even at high frequencies after sufficiently long times, which leads to the eventual emergence of ergodic behavior.

Finally, we note that unlike other quasi-periodically driven QKRs, there doesn't appear to exist any direct mapping between the FQKR discussed in this work and real space lattice systems. However, we leave this as an open problem for future endeavors. It may also be interesting to analyze the consequences of driving a kicked top with a similar Fibonacci drive.

ACKNOWLEDGMENTS

We acknowledge Markus Heyl for discussions and for his very useful comments and suggestions. Sourav Bhattacharjee acknowledges CSIR, India for financial support. Souvik Bandyopadhyay acknowledges financial support from PMRF, MHRD, India. AD acknowledges financial support from a SPARC program, MHRD, India and SERB, DST, New Delhi, India..

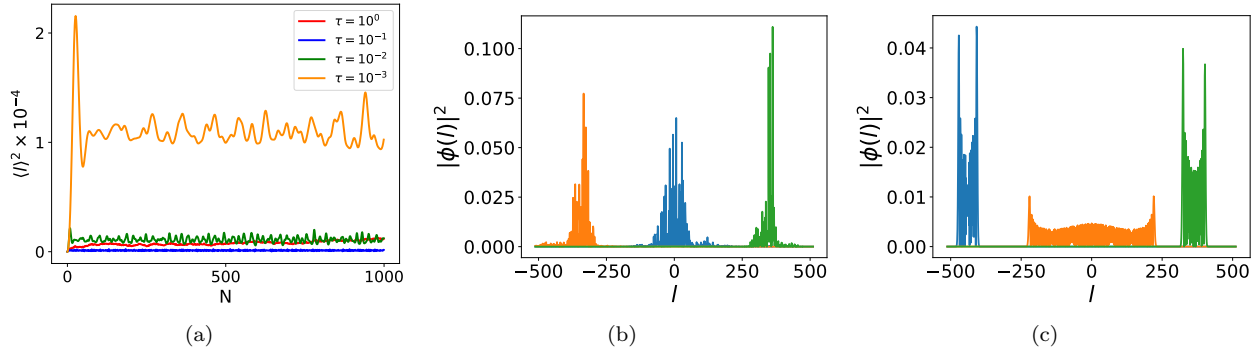


FIG. 4. (a) Evolution of the kinetic energy observed at stroboscopic instants N for a regular rotor, $\mathcal{K}_2 = 15$. The energy dynamically localizes for all driving frequencies, barring resonance conditions which are not considered in this work.

Appendix A: Regular quantum kicked rotor

The regular QKR is represented by the Hamiltonian,

$$H(t) = \frac{\hat{l}^2}{2I} + \mathcal{K} \cos \hat{\theta} \sum_{n=0}^{\infty} \delta(t - nT). \quad (\text{A1})$$

As discussed in the main text, the above Hamiltonian always exhibits dynamical localization, irrespective of the drive frequency (see Fig. 4(a)). The Floquet propagator governing the evolution of the rotor at stroboscopic instants is given by,

$$U_F = e^{-i\frac{\hat{l}^2}{2}\tau} e^{-i\mathcal{K} \cos \hat{\theta}}. \quad (\text{A2})$$

Let us consider the eigen-spectrum of the Floquet propagator: $U_F = \sum_m e^{i\phi_m} |\phi_m\rangle \langle \phi_m|$. As the Hilbert space dimension is infinite and the *quasi-energies* ϕ_m are defined modulo 2π , the Floquet propagator has a dense eigen-spectrum with ill-defined mean level spacing. However, as shown in Fig. 4(b), all the eigenstates $|\phi_m\rangle$ turn out to be exponentially localized in the angular momentum space, unless $\tau \ll 1$ which we shall consider shortly. To see how these properties lead to a dynamical localization in the dynamics, let us explicitly calculate the kinetic energy in terms of the matrix elements of the Floquet propagator. Without loss of generality, we assume that the rotor is initialized in a definite angular momentum state $|l_0\rangle$. The kinetic energy after N stroboscopic instants can then be evaluated as,

$$\begin{aligned} \langle \hat{l}^2 \rangle &= \langle l_0 | U_N^\dagger \hat{l}^2 U_N | l_0 \rangle \\ &= \sum_{l, m, m'} l^2 e^{iN(\phi_m - \phi_{m'})} V_{l_0 m'} V_{l m'}^* V_{l m} V_{l_0 m}^*, \end{aligned} \quad (\text{A3})$$

where $V_{l_0 m} = \langle l_0 | \phi_m \rangle$ and so on. As the eigenstates are exponentially localized in the angular momentum basis, we have $V_{ll'} \approx 0$ for $|l - l'| > l_s$, where l_s is the *localization length* and is a measure of the number of Floquet eigenstates which overlaps with each angular momentum state. It is thus clear that in the equation above, only a finite number of eigenstates can contribute to the sum,

resulting in the effective quasi-energy spectrum being discreet with a mean level spacing of $2\pi/l_s$.

The onset of dynamical localization can now be explained as follows. If $2\pi N/l_s \gg 1$, all the oscillating terms in Eq. (A3) vanish; the average kinetic energy evaluates to,

$$\langle \hat{l}^2 \rangle = \sum_{l, m} l^2 |V_{l_0 m}|^2 |V_{l m}|^2 \sim l_s^2 + l_0^2, \quad (\text{A4})$$

which is independent of N . Further, the Heisenberg time can also be roughly approximated from $2\pi N^*/l_s \approx 1$ or $N^* \sim l_s$. As the kinetic energy is known to follow the classical dynamics till N^* with a diffusion constant $\sim \mathcal{K}_{cl}^2 = \mathcal{K}^2 \tau^2$, we have

$$\langle \hat{l}^2 \rangle \sim \mathcal{K}^2 \tau^2 N^* + l_0^2. \quad (\text{A5})$$

or,

$$l_s^2 \sim \mathcal{K}^2 \tau^2 l_s, \quad (\text{A6})$$

which determines both the localization length and the Heisenberg time as,

$$l_s \sim \mathcal{K}^2 \tau^2. \quad (\text{A7})$$

If $\tau \ll 1$, an interesting situation arises. As the classical rotor exhibits no diffusive growth in the kinetic energy at low values of τ , the Heisenberg time is expected to vanish. This is indeed the case as can be easily seen from Eq. (A7) above. However, the Floquet eigenstates ‘broaden’ out in the angular momentum basis as can be seen by comparing Figs. 4(b) and 4(c), although they still remain highly localized. The broadening of the eigenstates is reflected in the mean kinetic energy, which then increases as τ is decreased further.

Finally, we remark on the ballistic growth seen in the kinetic energy at very short times, when $\tau \ll 1$ and $l_0 \approx 0$. To explain its origin, let us resolve the unitary operator U_n given in Eq. (A2) in the angular momentum basis,

$$\langle l' | U_F | l \rangle = (-i)^{l-l'} e^{-i\frac{\hat{l}^2}{2}\tau} J_{l-l'}(\mathcal{K}). \quad (\text{A8})$$

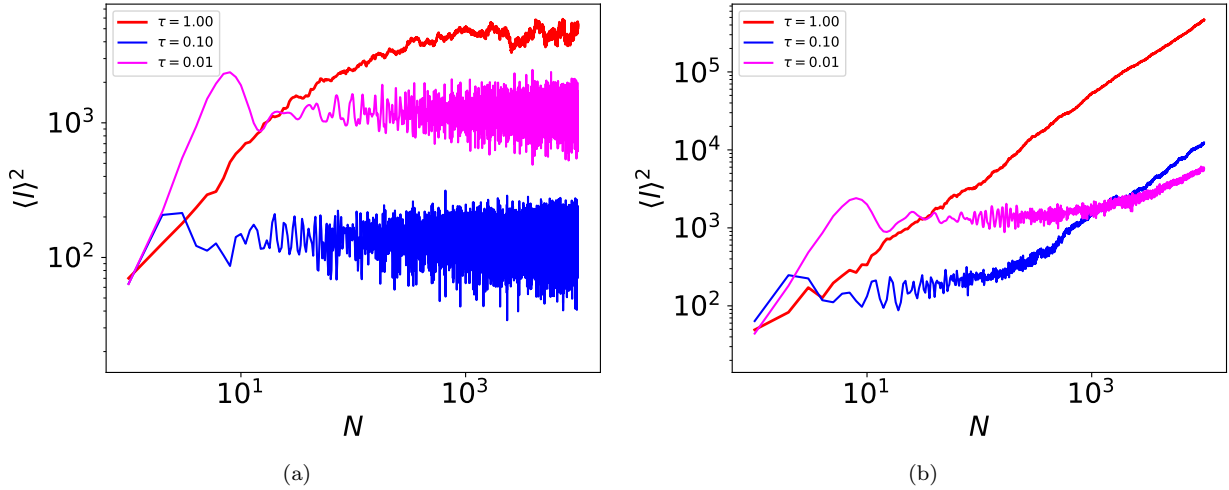


FIG. 5. (a) Evolution of the kinetic energy observed at stroboscopic instants N when the rotor is driven with (a) bi-periodic and (b) aperiodic binary sequences and the kick amplitudes chosen as $\mathcal{K}_1 = 10$ and $\mathcal{K}_2 = 12$. The energy saturates for all driving frequencies in the case of the bi-periodic sequence while it grows diffusively in the other case.

It is straightforward to see that if $\tau \ll$ and $l_0 \approx 0$, we

have $l_0^2\tau \approx 0$. The explicit wave-function of the rotor after q kicks is thus given by,

$$\psi(l) = (-1)^{l-l_0} \sum_{\{l_i\}} e^{-i\frac{l_0^2}{2}\tau} J_{l_0-l_1}(\mathcal{K}) e^{-i\frac{l_1^2}{2}\tau} J_{l_1-l_2}(\mathcal{K}) \cdots e^{-i\frac{l_{q-1}^2}{2}\tau} J_{l_{q-1}-l}(\mathcal{K}). \quad (\text{A9})$$

From our previous discussion, it is clear that $\max(l_i) = l_0 + il_s$, where $\max(l_i)$ is the maximum value of l_i which can contribute finitely to the sum in the above equation and l_s is the localization length defined in the preceding discussion. If q is not too large, we have $\max(l_i)^2\tau \approx 0$. The probability distribution of the rotor in the angular momentum basis can then be approximated as,

$$|\psi(l)|^2 = |J_{l-l_0}(q\mathcal{K})|^2. \quad (\text{A10})$$

Note that the situation is reminiscent of the (primary) resonance condition $\tau = 4\pi$, in which the kinetic energy grows ballistically throughout. In our case, the resonance like situation persists at small values of q when the rotor is driven with $\tau \ll 1$, thus explaining the initial ballistic growth seen in Fig. 4(a) (orange curve).

Appendix B: Dynamics of the rotor under bi-periodic and aperiodic sequences

Let us first consider the scenario where the rotor is kicked with a bi-periodic sequence, such that $(K_N)_{N=1}^{\infty} \equiv \mathcal{K}_1, \mathcal{K}_2, \mathcal{K}_1, \mathcal{K}_2, \dots$. Fig. 5(a) shows the evolution of $\langle l^2 \rangle$ as a function of stroboscopic instants N for different values of τ when the initial wave-packet is localized at $l_0 = 0$.

We find that $\langle l^2 \rangle$ saturates after an initial growth in all the cases. We have also checked numerically that the localization persists for all choices of $\mathcal{K}_1, \mathcal{K}_2$ and $\Delta\mathcal{K} = |\mathcal{K}_1 - \mathcal{K}_2|$.

As in the case of the regular rotor, the localization in the dynamics of the bi-periodic rotor can be easily explained from the properties of the appropriately constructed Floquet propagator. Noting that $H(t + 2\tau) = H(t)$ for the bi-periodic rotor, we define,

$$U_F^{\text{bi}} = e^{-i\frac{l^2}{2}\tau} e^{-i\mathcal{K}_2 \cos \hat{\theta}} e^{-i\frac{l^2}{2}\tau} e^{-i\mathcal{K}_1 \cos \hat{\theta}}, \quad (\text{B1})$$

as the Floquet propagator calculated over two stroboscopic time intervals. We have checked numerically that the eigenstates of U_F^{bi} are also exponentially localized in the angular momentum space. This, we recall from the discussion in Sec. II, is a sufficient condition for the onset of localization in the dynamics of the rotor.

The above situation completely changes if the rotor is kicked with a random binomial sequence where the amplitude of the kick can either be \mathcal{K}_1 or \mathcal{K}_2 with equal probability at every $t = NT$. This is illustrated in Fig. 5(b) which shows that rotor evolves diffusively, $\langle l^2 \rangle = DN$, irrespective of the driving frequency.

Appendix C: High frequency expansion of the unitary operator

In this section, we shall derive the high frequency expansion of the time-evolution unitary operator for a QKR when driven with a binary sequence of kicks. As discussed in Eq. (3) of the main text, the unitary operator driving tdriveshe evolution between the $(n-1)^{th}$ and n^{th} kicks is given by,

$$U_n = e^{-i\frac{\hat{l}^2}{2}\tau} e^{-iK_n \cos \hat{\theta}}. \quad (\text{C1})$$

We recall that given a pair of non-commuting operators A and B , one can write $e^A e^B = e^C$, where C is given by the Baker-Campbell-Hausdorff formula,

$$C = A + B + \frac{1}{2} [A, B] + \frac{1}{12} \left([A, [A, B]] + [B, [B, A]] \right) + \dots \quad (\text{C2})$$

Substituting $A = -i\hat{l}^2\tau/2$ and $B = -iK_n \cos \hat{\theta}$, it is straightforward to check that the only commutators in the above expression which contribute up to linear order in τ are,

$$[A, B] = -\frac{iK_n\tau}{2} \left(\hat{l} \sin \hat{\theta} + \sin \hat{\theta} \hat{l} \right) + \mathcal{O}(\tau^2) \quad (\text{C3a})$$

$$[B, [B, A]] = \frac{-iK_n^2\tau}{2} \sin^2 \hat{\theta} + \mathcal{O}(\tau^2). \quad (\text{C3b})$$

At high frequencies or $\tau \ll 1$, we can therefore neglect all other commutators in Eq. (C2). Recalling $K_n \in \{\mathcal{K}_1, \mathcal{K}_2\}$ for a binary sequence, we obtain,

$$U_n \approx e^{-iL_m}, \quad (\text{C4a})$$

$$L_m = \mathcal{K}_m \cos \hat{\theta} + \frac{\tau}{2} \left[\hat{l}^2 + \frac{\mathcal{K}_m}{2} \left(\hat{l} \sin \hat{\theta} + \sin \hat{\theta} \hat{l} \right) + \frac{\mathcal{K}_m^2}{6} \sin^2 \hat{\theta} \right] + \mathcal{O}(\tau^2), \quad (\text{C4b})$$

where $m = 1, 2$.

Let us now consider the evolution of the QKR when driven with a Fibonacci sequence of kicks. For $\tau \ll 1$ such that Eq. (C4) is satisfied, the evolution operator assumes the form,

$$U = \dots e^{-iL_2} e^{-iL_1} e^{-iL_2} e^{-iL_1} e^{-iL_2} e^{-iL_1} \quad (\text{C5})$$

Our purpose is to derive an approximate expression for the evolution operator of the form $U_N \approx e^{-iL_N}$ by progressively approximating the unitary operator for adjacent time intervals. Let us denote the evolution over the first two time intervals: $U_2 \approx e^{-iL_2} e^{-iL_1} = e^{-iL_{12}}$, where L_{12} is to be computed using the BCH formula. As before, we calculate the commutators,

$$[-iL_2, -iL_1] = i(\mathcal{K}_2 - \mathcal{K}_1) \frac{\tau}{2} \left(\hat{l} \sin \hat{\theta} + \sin \hat{\theta} \hat{l} \right) + \mathcal{O}(\tau^2), \quad (\text{C6a})$$

$$[-iL_1, [-iL_1, -iL_2]] = i\mathcal{K}_1 (\mathcal{K}_2 - \mathcal{K}_1) \tau \sin^2 \hat{\theta} + \mathcal{O}(\tau^2), \quad (\text{C6b})$$

$$[-iL_2, [-iL_2, -iL_1]] = -i\mathcal{K}_2 (\mathcal{K}_2 - \mathcal{K}_1) \tau \sin^2 \hat{\theta} + \mathcal{O}(\tau^2). \quad (\text{C6c})$$

It can be straightforwardly verified from the above expressions that all other higher order commutators, such as $[L_1, [L_1, [L_1, L_2]]]$, will contribute terms which are at least quadratic in order τ . Retaining terms up to linear order in τ , we find,

$$\begin{aligned} -iL_{12} &= -i\beta(2)L_2 - i\alpha(2)L_1 + \delta(2) [-iL_2, -iL_1] \\ &+ \eta_1(2) [-iL_1, [-iL_1, -iL_2]] + \eta_2(2) [-iL_2, [-iL_2, -iL_1]], \end{aligned}$$

where $\alpha(2) = \beta(2) = 1$, $\delta(2) = 1/2$ and $\eta_1(2) = \eta_2(2) = 1/12$.

We can now build the unitary operator as follows. After three kicks, the evolution operator can be approximated as $U_3 = e^{-iL_1} e^{-iL_{12}} = e^{-iL_{13}}$, where L_{13} is found to be,

$$\begin{aligned} -iL_{13} &= -2iL_1 - iL_2 - \frac{1}{6} [-iL_1, [-iL_1, -iL_2]] \\ &+ \frac{1}{6} [-iL_2, [-iL_2, -iL_1]]. \end{aligned} \quad (\text{C7})$$

A careful inspection reveals that when the N^{th} kick is \mathcal{K}_1 , the expansion coefficients obey the following recursion relations,

$$\delta(N) = \delta(N-1) - \frac{1}{2}\beta(N-1) \quad (\text{C8a})$$

$$\eta_1(N) = \eta_1(N-1) - \frac{1}{2}\delta(N-1) + \frac{1}{12}\beta(N-1) \left(1 - \alpha(N-1) \right) \quad (\text{C8b})$$

$$\eta_2(N) = \eta_2(N-1) + \frac{1}{12}\beta^2(N-1) \quad (\text{C8c})$$

Conversely, when the N^{th} kick is \mathcal{K}_2 , the recursion relations are given by,

$$\delta(N) = \delta(N-1) + \frac{1}{2}\alpha(N-1) \quad (\text{C9a})$$

$$\eta_1(N) = \eta_1(N-1) + \frac{1}{12}\alpha^2(N-1) \quad (\text{C9b})$$

$$\eta_2(N) = \eta_2(N-1) + \frac{1}{2}\delta(N-1) + \frac{1}{12}\alpha(N-1) \left(1 - \beta(N-1) \right) \quad (\text{C9c})$$

To verify the above recursion relations, we explicitly calculate L_{14} and L_{15} as in Eq. (C7),

$$\begin{aligned} -iL_{14} &= -3iL_1 - iL_2 - \frac{1}{2} [-iL_2, -iL_1] \\ &- \frac{1}{4} [-iL_1, [-iL_1, -iL_2]] + \frac{1}{4} [-iL_2, [-iL_2, -iL_1]], \end{aligned} \quad (\text{C10})$$

$$\begin{aligned}
-iL_{15} &= -3iL_1 - 2iL_2 + [-iL_2, -iL_1] \\
&\quad + \frac{1}{2} [-iL_1, [-iL_1, -iL_2]]. \quad (\text{C11})
\end{aligned}$$

We recall from Eq. (C5) that the fourth and fifth kicks in the Fibonacci sequence are \mathcal{K}_1 and \mathcal{K}_2 , respectively. Thus, the expansion coefficients in L_{14} and L_{15} satisfy the recursion relations given in Eqs. (C8) and (C9), respectively.

The recursion relations in Eqs. (C8) and (C9) can be unified using the generating function of the binary Fibonacci sequence, defined as,

$$\gamma(n) = \lfloor (n+1)G \rfloor - \lfloor nG \rfloor, \quad (\text{C12})$$

where $G = (\sqrt{5}+1)/2$ is the golden ratio and $\lfloor x \rfloor$ denotes the greatest integer less than or equal to x . For any positive integer n , $\gamma(n) \in \{1, 2\}$. The function $\gamma(n)-1$ is therefore a Boolean function and it generates the required Fibonacci sequence. We show this below by explicitly evaluating it for $n = 1, 2, 3, \dots, 13$,

n	1	2	3	4	5	6	7	8	9	10	11	12	13
$\gamma(n)-1$	1	0	1	1	0	1	0	1	1	0	1	1	0

Substituting K_1 and K_2 in place of 1 and 0 in the second row of the table above, we recover the Fibonacci sequence defined in Eq. (6) of the main text.

Using the generating function $\gamma(n)$ defined above, the coefficients $\beta(N)$ and $\alpha(N)$ are immediately evaluated as,

$$\beta(N) = \sum_{n=1}^N (2 - \gamma(n)), \quad (\text{C13a})$$

$$\alpha(N) = \sum_{n=1}^N (\gamma(n) - 1) = N - \beta(N). \quad (\text{C13b})$$

Having evaluated $\alpha(N)$ and $\beta(N)$, the recursion relation for $\delta(N)$ can be simplified to,

$$\delta(N) = \sum_{n=1}^N \left[(2 - \gamma(n)) \frac{\alpha(n-1)}{2} - (\gamma(n) - 1) \frac{\beta(n-1)}{2} \right], \quad (\text{C14})$$

where $\alpha(0) = \beta(0) = 0$. Further, it can be verified that if $\gamma(n) = 2$, then $\beta(n-1) = \lfloor n/(1+G) \rfloor$. Similarly, if $\gamma(n) = 1$, then $\alpha(n-1) = \lfloor nG/(1+G) \rfloor$. Substituting in the above expression, we therefore find,

$$\delta(N) = -\frac{1}{2} \sum_{n=1}^N \left[(\gamma(n) - 1)(n-1) - \left\lfloor \frac{nG}{1+G} \right\rfloor \right], \quad (\text{C15})$$

where we have used the relation $\lfloor nG/(1+G) \rfloor + \lfloor n/(1+G) \rfloor = n-1$. Finally, the coefficients $\eta_1(N)$ and $\eta_2(N)$ can be evaluated as (needs to be verified),

$$\begin{aligned}
\eta_1(N) &= \frac{1}{12} \sum_{m=1}^N \left[(2 - \gamma(n)) \left\lfloor \frac{nG}{1+G} \right\rfloor^2 \right. \\
&\quad \left. + (1 - \gamma(n)) \left(6\delta(n-1) - (2-n) \left\lfloor \frac{n}{1+G} \right\rfloor - \left\lfloor \frac{n}{1+G} \right\rfloor^2 \right) \right],
\end{aligned}$$

$$\begin{aligned}
\eta_2(N) &= \frac{1}{12} \sum_{m=1}^N \left[(\gamma(n) - 1) \left\lfloor \frac{n}{1+G} \right\rfloor^2 \right. \\
&\quad \left. + (2 - \gamma(n)) \left(6\delta(n-1) + (2-n) \left\lfloor \frac{nG}{1+G} \right\rfloor + \left\lfloor \frac{nG}{1+G} \right\rfloor^2 \right) \right],
\end{aligned}$$

[1] B. V. Chirikov, A universal instability of many-dimensional oscillator systems, *Physics Reports* **52**, 263 (1979).

[2] F. M. Izrailev, Simple models of quantum chaos: Spectrum and eigenfunctions, *Physics Reports* **196**, 299 (1990).

[3] G. Casati, B. V. Chirikov, F. M. Izrailev, and J. Ford, Stochastic behavior of a quantum pendulum under a periodic perturbation, in *Stochastic Behavior in Classical and Quantum Hamiltonian Systems*, edited by G. Casati and J. Ford (Springer Berlin Heidelberg, Berlin, Heidelberg, 1979) pp. 334–352.

[4] S. Fishman, D. R. Grempel, and R. E. Prange, Chaos, quantum recurrences, and anderson localization, *Phys. Rev. Lett.* **49**, 509 (1982).

[5] D. R. Grempel, R. E. Prange, and S. Fishman, Quantum dynamics of a nonintegrable system, *Phys. Rev. A* **29**, 1639 (1984).

[6] S.-J. Chang and K.-J. Shi, Evolution and exact eigenstates of a resonant quantum system, *Phys. Rev. A* **34**, 7 (1986).

[7] S. Fishman, D. R. Grempel, and R. E. Prange, Temporal crossover from classical to quantal behavior near dynamical critical points, *Phys. Rev. A* **36**, 289 (1987).

[8] S. Fishman, R. E. Prange, and M. Griniasty, Scaling theory for the localization length of the kicked rotor, *Phys. Rev. A* **39**, 1628 (1989).

[9] E. J. Galvez, B. E. Sauer, L. Moorman, P. M. Koch, and D. Richards, Microwave ionization of h atoms: Breakdown of classical dynamics for high frequencies, *Phys. Rev. Lett.* **61**, 2011 (1988).

[10] J. E. Bayfield, G. Casati, I. Guarneri, and D. W. Sokol,

Localization of classically chaotic diffusion for hydrogen atoms in microwave fields, Phys. Rev. Lett. **63**, 364 (1989).

[11] F. L. Moore, J. C. Robinson, C. Bharucha, P. E. Williams, and M. G. Raizen, Observation of dynamical localization in atomic momentum transfer: A new testing ground for quantum chaos, Phys. Rev. Lett. **73**, 2974 (1994).

[12] F. L. Moore, J. C. Robinson, C. F. Bharucha, B. Sundaram, and M. G. Raizen, Atom optics realization of the quantum δ -kicked rotor, Phys. Rev. Lett. **75**, 4598 (1995).

[13] H. Ammann, R. Gray, I. Shvarchuck, and N. Christensen, Quantum delta-kicked rotor: Experimental observation of decoherence, Phys. Rev. Lett. **80**, 4111 (1998).

[14] M. Bitter and V. Milner, Experimental observation of dynamical localization in laser-kicked molecular rotors, Phys. Rev. Lett. **117**, 144104 (2016).

[15] S. Sarkar, S. Paul, C. Vishwakarma, S. Kumar, G. Verma, M. Sainath, U. D. Rapol, and M. S. Santhanam, Non-exponential decoherence and subdiffusion in atom-optics kicked rotor, Phys. Rev. Lett. **118**, 174101 (2017).

[16] H.-J. Stockmann, *Quantum Chaos: An Introduction* (Cambridge University Press, 1999).

[17] F. Haake, S. Gnutzmann, and M. Kuš, *Quantum Signatures of Chaos*, 4th ed. (Springer International Publishing, 2018).

[18] L. D. Alessio, Y. Kafri, A. Polkovnikov, and M. Rigol, From quantum chaos and eigenstate thermalization to statistical mechanics and thermodynamics, Advances in Physics **65**, 239 (2016).

[19] P. W. Anderson, Absence of diffusion in certain random lattices, Phys. Rev. **109**, 1492 (1958).

[20] E. Abrahams, P. W. Anderson, D. C. Licciardello, and T. V. Ramakrishnan, Scaling theory of localization: Absence of quantum diffusion in two dimensions, Phys. Rev. Lett. **42**, 673 (1979).

[21] H. Lignier, J. Chabé, D. Delande, J. C. Garreau, and P. Sriftgiser, Reversible destruction of dynamical localization, Phys. Rev. Lett. **95**, 234101 (2005).

[22] G. Casati, I. Guarneri, and D. L. Shepelyansky, Anderson transition in a one-dimensional system with three incommensurate frequencies, Phys. Rev. Lett. **62**, 345 (1989).

[23] B. Gadway, J. Reeves, L. Krinner, and D. Schneble, Evidence for a quantum-to-classical transition in a pair of coupled quantum rotors, Phys. Rev. Lett. **110**, 190401 (2013).

[24] A. C. Keser, S. Ganeshan, G. Refael, and V. Galitski, Dynamical many-body localization in an integrable model, Phys. Rev. B **94**, 085120 (2016).

[25] P. Qin, A. Andreeanov, H. C. Park, and S. Flach, Interacting ultracold atomic kicked rotors: loss of dynamical localization, Sci. Rep. **7**, 2045 (2017).

[26] E. B. Rozenbaum and V. Galitski, Dynamical localization of coupled relativistic kicked rotors, Phys. Rev. B **95**, 064303 (2017).

[27] S. Notarnicola, F. Iemini, D. Rossini, R. Fazio, A. Silva, and A. Russomanno, From localization to anomalous diffusion in the dynamics of coupled kicked rotors, Phys. Rev. E **97**, 022202 (2018).

[28] S. Notarnicola, A. Silva, R. Fazio, and A. Russomanno, Slow heating in a quantum coupled kicked rotors system, J. Stat. Mech. , 024208 (2020).

[29] A. Russomanno, M. Fava, and R. Fazio, Chaos and subdiffusion in infinite-range coupled quantum kicked rotors, Phys. Rev. B **103**, 224301 (2021).

[30] E. Ott, T. M. Antonsen, and J. D. Hanson, Effect of noise on time-dependent quantum chaos, Phys. Rev. Lett. **53**, 2187 (1984).

[31] I. Guarneri, Energy growth in a randomly kicked quantum rotator, Lettere al Nuovo Cimento (1971-1985) **40**, 171 (1984).

[32] S. Brouard and J. Plata, Quantum -kicked rotor: the effect of amplitude noise on the quantum resonances, Journal of Physics A: Mathematical and General **36**, 3745 (2003).

[33] B. G. Klappauf, W. H. Oskay, D. A. Steck, and M. G. Raizen, Observation of noise and dissipation effects on dynamical localization, Phys. Rev. Lett. **81**, 1203 (1998).

[34] D. A. Steck, V. Milner, W. H. Oskay, and M. G. Raizen, Quantitative study of amplitude noise effects on dynamical localization, Phys. Rev. E **62**, 3461 (2000).

[35] H. Schomerus and E. Lutz, Nonexponential decoherence and momentum subdiffusion in a quantum lévy kicked rotator, Phys. Rev. Lett. **98**, 260401 (2007).

[36] G. Floquet, Sur les équations différentielles linéaires à coefficients périodiques, Annales scientifiques de l'Ecole Normale Supérieure **12**, 47 (1883).

[37] J. H. Shirley, Solution of the schrödinger equation with a hamiltonian periodic in time, Phys. Rev. **138**, B979 (1965).

[38] M. Bükov, L. D'Alessio, and A. Polkovnikov, Universal high-frequency behavior of periodically driven systems: from dynamical stabilization to floquet engineering, Advances in Physics **64**, 139 (2015).

[39] A. Eckardt, Colloquium: Atomic quantum gases in periodically driven optical lattices, Rev. Mod. Phys. **89**, 011004 (2017).

[40] I. Martin, G. Refael, and B. Halperin, Topological frequency conversion in strongly driven quantum systems, Phys. Rev. X **7**, 041008 (2017).

[41] A. Thue, Über unendliche zeichenreihen, Norske Vidensk. Selsk. Skr. I **7**, 1 (1906).

[42] H. M. Morse, Recurrent geodesics on a surface of negative curvature, Trans. Am. Math. Soc. **22**, 84 (1921).

[43] H. M. Morse, A one-to-one representation of geodesics on a surface of negative curvature, Am. J. Math. **43**, 33 (1921).

[44] S. Nandy, A. Sen, and D. Sen, Aperiodically driven integrable systems and their emergent steady states, Phys. Rev. X **7**, 031034 (2017).

[45] P. T. Dumitrescu, R. Vasseur, and A. C. Potter, Logarithmically slow relaxation in quasiperiodically driven random spin chains, Phys. Rev. Lett. **120**, 070602 (2018).

[46] S. Nandy, A. Sen, and D. Sen, Steady states of a quasiperiodically driven integrable system, Phys. Rev. B **98**, 245144 (2018).

[47] S. Maity, U. Bhattacharya, A. Dutta, and D. Sen, Fibonacci steady states in a driven integrable quantum system, Phys. Rev. B **99**, 020306 (2019).

[48] B. Mukherjee, A. Sen, D. Sen, and K. Sengupta, Restoring coherence via aperiodic drives in a many-body quantum system, Phys. Rev. B **102**, 014301 (2020).

[49] P. Zhang and Y. Gu, Periodically and Quasi-periodically Driven Dynamics of Bose-Einstein Condensates, SciPost Phys. **9**, 79 (2020).

[50] H. Zhao, F. Mintert, R. Moessner, and J. Knolle, Ran-

dom multipolar driving: Tunably slow heating through spectral engineering, *Phys. Rev. Lett.* **126**, 040601 (2021).

[51] S. Ray, S. Sinha, and D. Sen, Dynamics of quasiperiodically driven spin systems, *Phys. Rev. E* **100**, 052129 (2019).

[52] S. Ostlund, R. Pandit, D. Rand, H. J. Schellnhuber, and E. D. Siggia, One-dimensional schrödinger equation with an almost periodic potential, *Phys. Rev. Lett.* **50**, 1873 (1983).

[53] M. Kohmoto, L. P. Kadanoff, and C. Tang, Localization problem in one dimension: Mapping and escape, *Phys. Rev. Lett.* **50**, 1870 (1983).

[54] B. Sutherland, Simple system with quasiperiodic dynamics: a spin in a magnetic field, *Phys. Rev. Lett.* **57**, 770 (1986).

[55] J. Ringot, P. Sriftgiser, J. C. Garreau, and D. Delande, Experimental evidence of dynamical localization and delocalization in a quasiperiodic driven system, *Phys. Rev. Lett.* **85**, 2741 (2000).

[56] P. T. Dumitrescu, R. Vasseur, and A. C. Potter, Logarithmically slow relaxation in quasiperiodically driven random spin chains, *Phys. Rev. Lett.* **120**, 070602 (2018).